Lethaia
AN INTERNATIONAL JOURNAL OF PALAEONTOLOGY AND STRATIGRAPHY

Eigenshape analysis of ammonoid sutures

TAKAO UBUKATA, KAZUSHIGE TANABE, YASUNARI SHIGETA, HARUYOSHI MAEDA AND ROYAL H. MAPES

LETHAIA

Ubukata, T., Tanabe, K., Shigeta, Y., Maeda, H. & Mapes, R.H. 2010: Eigenshape analysis of ammonoid sutures. *Lethaia*, Vol. 43, pp. 266–277.

A morphometric method based on eigenshape analysis is proposed for characterizing the morphospace of widely varied ammonoid suture shapes. The analysis requires initially the placement of a suture line in an *x*–*y* coordinate system, with the ventral and umbilical extremes located on the *x*-axis. Series of *x*- and *y*-coordinates along the suture line are used as descriptors. The coordinate data are summarized into the two largest principal components using eigenshape analysis. A total of 115 species belonging to six ammonoid orders, spanning from the Devonian to the Cretaceous, was utilized in the present analysis. The analysis, using *y*-coordinate data, revealed differences in morphological variation in suture shape among taxa within the Mesozoic ammonitids: the Lytoceratina and Ammonitina were characterized by small negative values of the first eigenshape scores, whereas the Phylloceratina (the sister group of the Lytoceratina plus Ammonitina), as well as the Triassic ceratitids and Palaeozoic ammonoids, have a wide range of the first eigenshape scores. The pattern of data obtained from many different ammonoid species, as plotted on eigenshape axes in the morphospace constructed based on *y*-coordinate data, reveals a plesiomorphic aspect of suture shape in some phylloceratine species with respect to other ammonitids. □ *Ammonoids*, *eigenshape analysis*, *morphometrics*, *suture line*.

Takao Ubukata [sbtubuk@ipc.shizuoka.ac.jp], Institute of Geosciences, Shizuoka University, Oya 836, Surugaku, Shizuoka 422-8529, Japan; Kazushige Tanabe [tanabe@eps.s.u-tokyo.ac.jp], Department of Earth and Planetary Science, University of Tokyo, Hongo 7-3-1, Bunkyouku, Tokyo 113-0033, Japan; Yasunari Shigeta [shigeta@kahaku.go.jp], Department of Geology, National Science Museum, Hyakunincho 3-23-1, Shinjukuku, Tokyo 169-0073, Japan; Haruyoshi Maeda [maeda@kueps.kyoto-u.ac.jp], Department of Geology and Mineralogy, Kyoto University, Kitashirakawa-Oiwakecho, Sakyouku, Kyoto 606-8502, Japan; Royal H. Mapes [mapes@ohio.edu], Department of Geological Sciences, Ohio University, Athens, OH 45701, USA; *manuscript received on 01/05/2009; manuscript accepted on 22/06/2009.*

The ammonoid suture has long been a subject of palaeontologists' attention because of its great taxonomic utility (Arkell 1957; Miller *et al.* 1957; Kullmann & Wiedmann 1970; Wiedmann & Kullmann 1981; Korn & Klug 2002; Korn *et al.* 2003; Shevyrev 2006), morphogenetic wonder (Seilacher 1975; Westermann 1975; Bayer 1978; García-Ruiz *et al.* 1990; Hewitt *et al.* 1991; Hammer 1999) and puzzling functional morphology (Westermann 1958, 1975; Henderson 1984; Hewitt & Westermann 1986, 1987, 1997; Jacobs 1990; Weitschat & Bandel 1991; Olóriz & Palmqvist 1995; Saunders 1995; Seilacher & LaBarbera 1995; Saunders & Work 1996, 1997; Daniel *et al.* 1997; Olóriz *et al.* 1997; Hassan *et al.* 2002; Lewy 2002; Pérez-Claros 2005; Pérez-Claros *et al.* 2007; De Blasio 2008). The suture is the curved line of intersection between the external shell wall and a series of septa that partition the phragmocone internally into phragmocone chambers. Each suture consists of backward convex or concave folds that are termed lobes and saddles respectively. The lobes are classified into several categories according to their primary positions. The pattern of their arrangement, as well as nature of its ontogenetic change, is used as a taxonomic characteristic of ammonoids (Arkell 1957; Kullmann & Wiedmann 1970; Lehmann 1981; Wiedmann & Kullmann 1981; Korn & Klug 2002; Korn *et al.* 2003; Shevyrev 2006).

Many studies have sought to numerically quantify the suture geometry for the purpose of taxonomic comparison and functional morphological analysis. Most studies have adopted a mathematical representation of suture complexity using simple indices (Westermann 1971; Ward 1980; Jacobs 1990; Batt 1991; Saunders 1995; Saunders & Work 1996, 1997; Saunders *et al.* 1999; Ballantine 2007) or the fractal dimension (García-Ruiz *et al.* 1990; Boyajian & Lutz 1992; Lutz & Boyajian 1995; Olóriz & Palmqvist 1995; Checa & García-Ruiz 1996; Olóriz *et al.* 2002; Pérez-Claros *et al.* 2002; Pérez-Claros 2005); however, such approaches rely upon proxies of suture complexity rather than descriptors of the suture shape itself.

10.1111/j.1502-3931.2009.00191.x

One promising approach to provide a unique definition of suture shape is Fourier- or wavelet-based methods in which a periodic function describing the suture shape is decomposed into frequency and/or location domains (Canfield & Anstey 1981; Gildner 2003; Allen 2006, 2007); however, such an approach generally yields a large number of coefficients in representing the shape of interest, meaning that an additional multivariate analysis is required for the ordination of a population of shapes in the morphospace. A pattern matching technique using geographic information systems (Manship 2004) appears to be useful for the identification of suture patterns, although it provides a measure of the difference between sutures rather than a descriptor of suture shape itself.

In the present study, we propose an alternative approach to the quantitative description of suture shape based on an eigenshape analysis originally developed by Lohmann (1983). This method is designed to characterize the morphospace of a wide variety of ammonoid suture forms. The occupation pattern in the morphospace is compared among taxonomic groups to assess phylogenetic aspects of morphometric data on suture shape.

Materials and methods

Measurements of suture lines

We studied 128 specimens from 115 species belonging to six orders ranging in age from the Devonian to the Cretaceous (Table 1). The higher taxonomy follows Korn & Klug (2002) for Devonian ammonoids, Becker & Kullmann (1996) for Carboniferous to Permian ammonoids, Tozer (1981) for Triassic ammonoids, and Arkell *et al.* (1957) and Wright *et al.* (1996) for Jurassic and Cretaceous ammonitids. All the examined specimens are housed in the University Museum of the University of Tokyo (UMUT), Ohio University (OUZ) or Shizuoka University (SUM).

A piece of external hemi-suture was analysed for each sub-adult individual. To capture an image of the suture line, each portion of the external surface of each specimen (from which the shell wall had been removed) was photographed using a Keyence VH-5000 CCD camera, viewed perpendicular to the specimen surface (Ubukata 2004). Captured images were pieced together to form a synthetic image of the external hemi-suture, using Justsystem Hanako Photo-Retouch software on a personal computer. A series of x- and y-coordinates digitized along the suture line was translated, rotated and scaled in the x–y coordinate system such that the ventral and umbilical extremes were placed on the x-axis, separated by 10 000 pixels (Fig. 1A). Next, 4096 equally spaced points were interpolated along the series of normalized coordinate points using a cubic spline.

Eigenshape analysis of ammonoid sutures

To summarize the coordinate data into a small number of principal components, a modified version of eigenshape analysis was applied to the descriptors. The eigenshape analysis performs well with a variety of organic shapes that include not only closed outlines but also open curves (MacLeod 1999). The original eigenshape analysis is based on a series of angular deviations between adjacent coordinate points as a function of arc length along the object outline – an approach that is called 'Zahn and Roskies' function' (Zahn & Roskies 1972; Lohmann 1983). However, this function represents differences between adjacent points and is readily distorted by high-frequency noise, especially in the analysis of an intricate curve such as an ammonite suture. Accordingly, in the present case we employed a series of normalized and equally spaced x- and y-coordinate data as descriptors for eigenshape analysis. As a series of x-coordinates is not a periodic function but logically increases with increasing distance from the venter (Fig. 1C), such series were detrended by subtracting the expected linear increase in x to introduce periodicity to the x function (x'; see Fig. 1D). A series of normalized, equally spaced and/or detrended x'- or y-coordinate data for the kth individual is tentatively notated by z:

$$\mathbf{z}_k = (z_{k,1}, z_{k,2}, \ldots, z_{k,4096}).$$

Principal components were computed by singular value decomposition of interobject covariances of the descriptors of each set of z data for the ith point:

$$\mathbf{z}'_i = (z_{1,i}, z_{2,i}, \ldots, z_{n,i}),$$

where n is the total number of individuals (i.e. $n = 128$ in the present case). The jth eigenshape ($\omega_{i,j}$) for the ith point was calculated as an inner product between $\mathbf{z}'_i$ and the eigenvector of the covariance matrix ($\mathbf{v}_j$) divided by the corresponding jth largest singular value (μ_j):

$$\omega_{j,i} = \frac{\mathbf{z}'_i \cdot \mathbf{v}_j}{\mu_j}.$$

A series of the eigenshapes for individual points makes up the jth eigenshape vector:

Table 1. List of examined specimens.

Species	Specimens	Age	Locality
Agoniatitida			
Agoniatitina			
Latanarcestes sp.	UMUT-PM-29049	Devonian	Taouz, Morocco
Fidelites sp.	UMUT-PM-29050	Devonian	Erfoud, Morocco
Achguigites sp.	UMUT-PM-29051	Devonian	Erfoud, Morocco
Gephuroceratina			
Psedoprobeloceras costulatum	UMUT-PM-30079	Devonian	Taouz, Morocco
Beloceras sp.	UMUT-PM-29053	Devonian	Erfoud, Morocco
Anarcestina			
Anarcestes sp.1	UMUT-PM-30080	Devonian	Erfoud, Morocco
Anarcestes sp.2	UMUT-PM-30081	Devonian	Erfoud, Morocco
Praewerneroceras hollardi	OUZ-5600	Devonian	Taouz, Morocco
Pharciceratina			
Stenopharciceras sp.	UMUT-PM-29058	Devonian	Taouz, Morocco
Stenopharciceras lunulicosta	UMUT-PM-30082	Devonian	Taouz, Morocco
Synpharciceras clavilobum	UMUT-PM-30083	Devonian	Taouz, Morocco
Goniatitida			
Tornoceratina			
Epitornoceras mithracoides	UMUT-PM-29060	Devonian	Taouz, Morocco
Epitornoceras mithracoides	UMUT-PM-30084	Devonian	Taouz, Morocco
Phoenixites aff. *frechi*	UMUT-PM-30085	Devonian	Taouz, Morocco
Cheiloceras undulosum	UMUT-PM-30086	Devonian	Taouz, Morocco
Sporadoceras sp.	UMUT-PM-29064	Devonian	Taouz, Morocco
Sporadoceras muensteri	UMUT-PM-30087	Devonian	Erfoud, Morocco
Imitoceras rotatorium	OUZ-5601	Carboniferous	Rockford, Indiana
Goniatitina			
Girtyoceras meslerianum	OUZ-5602	Carboniferous	Jackforth Creek, Oklahoma
Eumorphoceras bisulcatum	OUZ-5603	Carboniferous	Leslie, Searcy Co., Arkansas
Hudsonoceras proteum	UMUT-PM-30088	Carboniferous	Knockauns Mts, Clare Co., Ireland
Goniatites aff. *crenistria*	UMUT-PM-29069	Carboniferous	Jackforth Creek, Oklahoma
Goniatites multiliratum	UMUT-PM-29070	Carboniferous	Jackforth Creek, Oklahoma
Perrinites hilli	UMUT-PM-30089	Permian	Las Pelicias, Coahuita, Mexico
Cravenoceras hesperium	OUZ-5604	Carboniferous	Death Valley, California
Neodimorphoceras sp.	OUZ-5605	Carboniferous	Texas
Cymoceras sp.	OUZ-5606	Carboniferous	Fayetteville, Washington Co., Arkansas
Glaphyrites clinei	UMUT-PM-30090	Carboniferous	Collinsville, Oklahoma
Syngastrioceras oblatum	OUZ-5607	Carboniferous	Fayetteville, Washington Co., Arkansas
Homoceras smithi	OUZ-5608	Carboniferous	Knockauns Mts, Clare Co., Ireland
Bisatoceras sp.	UMUT-PM-30091	Carboniferous	Oklahoma
Bisatoceras primum	OUZ-5609	Carboniferous	Oklahoma
Thalassoceras gemmellaroi	UMUT-PM-29078	Permian	Actasty R., S. Ural, Kazakhstan
Pseudoparalegoceras kesslerense	OUZ-5610	Carboniferous	Winslow, Washington Co., Arkansas
Wellerites mohri	OUZ-5611	Carboniferous	Carroll, Ohio
Goniolloboceras sp.	OUZ-5612	Carboniferous	South Bend, Texas
Mescalites sp.	OUZ-5613	Permian	Tularosa, New Mexico
Wewokites sp.	UMUT-PM-30092	Carboniferous	Oklahoma
Crimites subkrotowi	UMUT-PM-30093	Permian	Actasty R., S. Ural, Kazakhstan
Peritrochia typicus	UMUT-PM-29080	Permian	Actasty R., S. Ural, Kazakhstan
Peritrochia typicus	UMUT-PM-30094	Permian	Actasty R., S. Ural, Kazakhstan
Peritrochia invaribilis	UMUT-PM-30095	Permian	Actasty R., S. Ural, Kazakhstan
Uraloceras involutum	UMUT-PM-30096	Permian	Actasty R., S. Ural, Kazakhstan
Popanoceras annae	UMUT-PM-30097	Permian	Actasty R., S. Ural, Kazakhstan
Clymeniida			
Cyrtoclymeniina			
Cymaclymenia sp.1	UMUT-PM-29089	Devonian	Morocco
Cymaclymenia sp.2	UMUT-PM-29090	Devonian	Morocco
Clymeniina			
Platyclymenia sp.1	UMUT-PM-29091	Devonian	Morocco
Platyclymenia sp.2	UMUT-PM-29092	Devonian	Morocco
Oxyclymenia sp.	UMUT-PM-29094	Devonian	Morocco
Gonioclymenia sp.	UMUT-PM-30098	Devonian	Erfoud, Morocco
Prolecanitida			
Boesites sp.	UMUT-PM-30099	Carboniferous	Rochelle, Texas
Daraelites elegans	UMUT-PM-29097	Permian	Actasty R., S. Ural, Kazakhstan
Akmilleria electraensis	UMUT-PM-29098	Permian	White Pine Co., Nevada
Medlicottia intermedia	UMUT-PM-29099	Permian	Actasty R., S. Ural, Kazakhstan
Neopronorites skvorzovi	UMUT-PM-29100	Permian	Actasty R., S. Ural, Kazakhstan
Pseudopronorites arkansiensis	OUZ-5614	Carboniferous	Woolsey, Arkansas

Table 1. (Continued).

Species	Specimens	Age	Locality
Ceratitida			
Xenoceltites subevolutus	UMUT-MM-29103	Triassic	Spitsbergen, Norway
Xenoceltites subevolutus	UMUT-MM-30100	Triassic	Wallenbergfjellet, Spitsbergen, Norway
Paraceltites elegans	UMUT-PM-29101	Permian	Gaudalupe Mts., Texas
Dinartes asiaticus	UMUT-MM-30101	Triassic	Mangyshlak, Dolnapa, Kazakhstan
Pseudosageceras sp.	UMUT-MM-29104	Triassic	Spitsbergen, Norway
Amphipopanoceras cf. *medium*	UMUT-MM-30102	Triassic	Spitsbergen, Norway
Paranannites spathi	UMUT-MM-29106	Triassic	Criienden Spring, Nevada
Paranannites spathi	UMUT-MM-30103	Triassic	Stensiö-Fiellet, Spitsbergen, Norway
Paranannites aspenensis	UMUT-MM-30104	Triassic	Criienden Spring, Nevada
Prosphingites czekanowskii	UMUT-MM-30105	Triassic	Olenek River, Mengilach, Russia
Meekoceras graciliatus	UMUT-MM-30106	Triassic	Criienden Spring, Nevada
Boreomeekoceras keyserlingi	UMUT-MM-30107	Triassic	Olenek River, Mengilach, Russia
Arctoprionites nodosus	UMUT-MM-30108	Triassic	Stensiö-Fiellet, Spitsbergen, Norway
Dieneroceras spathi	UMUT-MM-30109	Triassic	Criienden Spring, Nevada
Arctoceras blomstrandi	UMUT-MM-30110	Triassic	Spitsbergen, Norway
Nordophiceras schmidti	UMUT-MM-30111	Triassic	Olenek River, Mengilach, Russia
Wasatchites tridentinus	UMUT-MM-30112	Triassic	Botheheia, Spitsbergen, Norway
Wasatchites tardus	UMUT-MM-30113	Triassic	Spitsbergen, Norway
Ceratites nodosus	UMUT-MM-30114	Triassic	Würzburg, Germany
Anagymnotoceras varium	UMUT-MM-30115	Triassic	Wallenbergfjellet, Spitsbergen, Norway
Favreticeras wallacei	UMUT-MM-29117	Triassic	McCoy Mine, Nevada
Stolleyites tenuis	UMUT-MM-29119	Triassic	Spitsbergen, Norway
Olenekoceras middendorffi	UMUT-MM-30116	Triassic	Olenek River, Mengilach, Russia
Olenikites spiniplicatus	UMUT-PM-30117	Triassic	Olenek River, Mengilach, Russia
Svalbardiceras spitsbergense	UMUT-PM-30118	Triassic	Wallenbergfjellet, Spitsbergen, Norway
Arctohungarites triformis	UMUT-PM-30119	Triassic	Olenek Bay, Laptev Sea, Russia
Lenotropites caurus	UMUT-PM-30120	Triassic	West Humboldt Range, Nevada
Pseudosvalbardiceras sibiricum	UMUT-PM-30121	Triassic	Olenek River, Mengilach, Russia
Ammonitida			
Phylloceratina			
Phylloceras consanguineans	UMUT-MM-29121	Jurassic	Sakaraha, Madagascar
Phylloceras sp.	UMUT-MM-29122	Cretaceous	Mahajang, Madagascar
Holcophylloceras sp.	UMUT-MM-29123	Jurassic	Sakaraha, Madagascar
Calliphylloceras sp.	UMUT-MM-29124	Jurassic	Sakaraha, Madagascar
Ptychophylloceras sp.	UMUT-MM-29125	Jurassic	Sakaraha, Madagascar
Phyllopachyceras ezoense	UMUT-MM-29126	Cretaceous	Saku, Hokkaido, Japan
Phyllopachyceras ezoense	UMUT-PM-30122	Cretaceous	Saku, Hokkaido, Japan
Hypophylloceras subramosum	UMUT-PM-30123	Cretaceous	Saku, Hokkaido, Japan
Hypophylloceras subramosum	UMUT-PM-30124	Cretaceous	Saku, Hokkaido, Japan
Tragophylloceras ibex	UMUT-MM-29130	Jurassic	Osuabrük, Germany
Lytoceratina			
Pterolytoceras sp.	UMUT-MM-29131	Jurassic	Sakaraha, Madagascar
Argonauticeras sp.	UMUT-MM-29132	Cretaceous	Mahajang, Madagascar
Tetragonites glabrus	UMUT-PM-30125	Cretaceous	Saku, Hokkaido, Japan
Tetragonites glabrus	UMUT-MM-29134	Cretaceous	Tappu, Hokkaido, Japan
Tetragonites popetensis	UMUT-PM-30126	Cretaceous	Saku, Hokkaido, Japan
Eotetragonites sp.	UMUT-MM-29136	Cretaceous	Mahajang, Madagascar
Gaudryceras striatum	SUM-RC-MM004	Cretaceous	Saku, Hokkaido, Japan
Gaudryceras striatum	UMUT-PM-30127	Cretaceous	Saku, Hokkaido, Japan
Gaudryceras tenuiliratum	UMUT-PM-30128	Cretaceous	Saku, Hokkaido, Japan
Gaudryceras sp.	UMUT-PM-30129	Cretaceous	Saku, Hokkaido, Japan
Gaudryceras sp.	UMUT-PM-30130	Cretaceous	Saku, Hokkaido, Japan
Ammonitina			
Grammoceras doerntense	UMUT-MM-29147	Jurassic	Döruten, Germany
Hecticoceras sp.	SUM-RC-MM020	Jurassic	Saltwick Nab, Yorkshire, England
Taramelliceras sp.	UMUT-MM-29149	Jurassic	Sakaraha, Madagascar
Lissoceras sp.	UMUT-MM-29150	Jurassic	Sakaraha, Madagascar
Grossouvria sp.	UMUT-MM-29152	Jurassic	Sakaraha, Madagascar
Aspidoceras sp.	UMUT-MM-29153	Jurassic	Sakaraha, Madagascar
Euaspidoceras sp.	UMUT-MM-29154	Jurassic	Sakaraha, Madagascar
Craspedites subditus	UMUT-PM-30131	Jurassic	Iwanowa, Russia
Desmoceras latidorsatum	UMUT-MM-29156	Cretaceous	Mahajang, Madagascar
Tragodesmoceroides subcostatus	UMUT-MM-29157	Cretaceous	Tappu, Hokkaido, Japan
Damesites semicostatus	UMUT-PM-30132	Cretaceous	Kotanbetsu, Hokkaido, Japan
Damesites sp.	UMUT-MM-29158	Cretaceous	Saku, Hokkaido, Japan
Hauericeras angustum	SUM-RC-MM006	Cretaceous	Saku, Hokkaido, Japan
Hauericeras angustum	UMUT-PM-30135	Cretaceous	Tappu, Hokkaido, Japan

Table 1. (Continued).

Species	Specimens	Age	Locality
Puzosia sp.	UMUT-MM-29162	Cretaceous	Mahajang, Madagascar
Yokoyamaoceras ishikawai	UMUT-MM-29164	Cretaceous	Saku, Hokkaido, Japan
Yokoyamaoceras ishikawai	UMUT-PM-30136	Cretaceous	Saku, Hokkaido, Japan
Cleoniceras besairiei	UMUT-MM-29167	Cretaceous	Mahajang, Madagascar
Anapachydiscus naumanni	UMUT-MM-29168	Cretaceous	Saku, Hokkaido, Japan
Teshioites ryugasensis	UMUT-MM-29169	Cretaceous	Saku, Hokkaido, Japan
Canadoceras kosmatti	UMUT-PM-30133	Cretaceous	Saku, Hokkaido, Japan
Canadoceras kosmatti	UMUT-PM-30134	Cretaceous	Saku, Hokkaido, Japan
Neogastroplites muelleri	UMUT-MM-29171	Cretaceous	Teigen, Petroleum Co., Montana

$$\boldsymbol{\omega}_j = (\omega_{j,1}, \omega_{j,2}, \ldots, \omega_{j,4096}).$$

The covariance between the *j*th eigenshape vector ($\boldsymbol{\omega}_j$) and each shape function ($\mathbf{z}_k$) defines the *j*th eigenshape score (=the principal component score) of each suture shape. All specimens listed in Table 1 were analysed together to obtain the first and second eigenshape scores.

Synthetic models of the x' and y functions can be generated along each eigenshape axis to visualize the variation in each component. Synthetic models for the first (E_1) and second (E_2) eigenshape scores are, respectively, given by

$$\mathbf{z}_1^* = E_1\boldsymbol{\omega}_1$$

and

$$\mathbf{z}_2^* = \overline{\mathbf{z}_1^*} + E_2\boldsymbol{\omega}_2.$$

Synthetic models along eigenshape axes were reproduced to assist in the geometric interpretation of the analytical results.

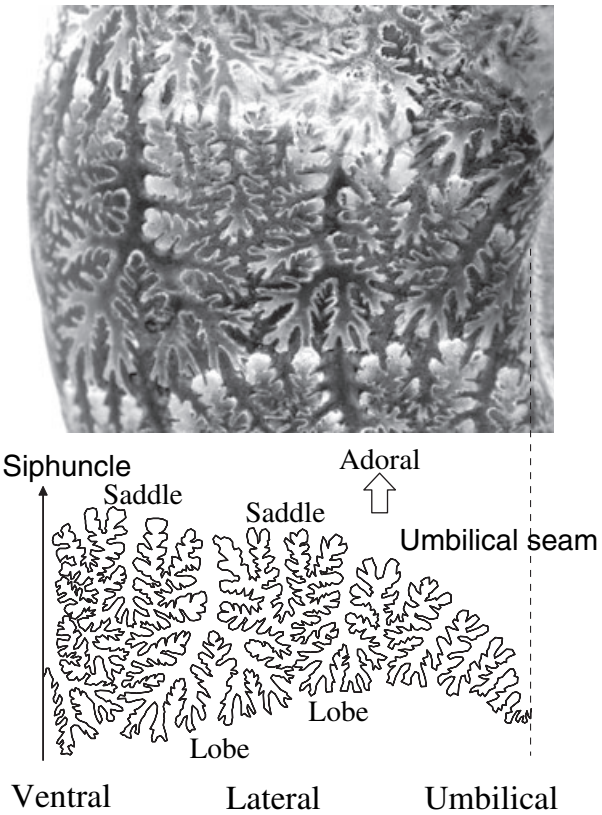

Fig. 1. A lateral view of an ammonoid whorl and trace of a suture line showing terminology on major suture elements in relation to the parts of the shell.

Results

The eigenshape scores obtained using all of the studied specimens are plotted in Figures 2, 3, with the data subdivided into the following three groups: agoniatitids, goniatitids and clymeniids (Figs 2A, 3A), prolecanitids and ceratitids (Figs 2B, 3B) and ammonitids (Figs 2C, 3C).

Analysis of the y *function*

The first and second eigenshapes (ES1 and ES2) account for 34.6% and 20.9% of the total variance respectively. Synthetic models of the y function reconstructed along the eigenshape axes indicate that both ES1 and ES2 reflect the difference among individuals of the shape of the first-order suture elements (Fig. 2D). As E_1 proceeds in the positive direction along the ES1 axis, the left-hand portion of the synthetic model becomes strongly concaved (E_1 maximum in Fig. 2D); i.e. a wide lobe tends to develop in the ventro-lateral area of the shell. By contrast, an individual with a negative E_1 tends to form a prominent saddle in the ventro-lateral region (E_1 minimum in Fig. 2D), as typically observed in the Lytoceratina and Ammonitina. Positive perturbations associated with ES2 represent the development of a wide lateral lobe lying slightly toward the venter (E_2 maximum in Fig. 2D), whereas the same portion is dominated by a

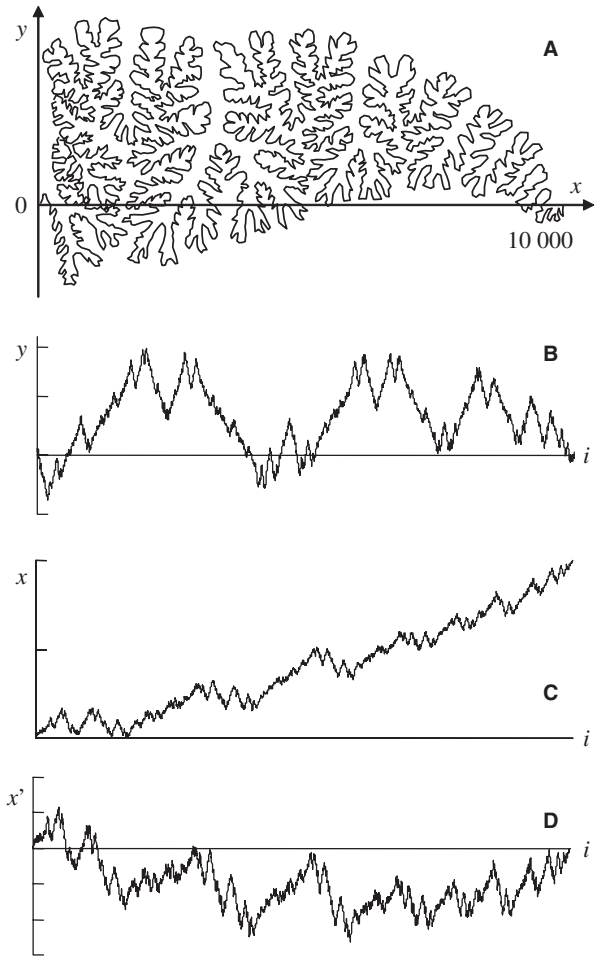

Fig. 2. Measurements of coordinate data along a suture line. A digitized suture line was placed in a reference system such that its ventral and umbilical extremes were located on the *x*-axis, separated by 10 000 pixels (A). A series of *y*-coordinate values measured along the suture line represents a periodic function of the cumulative chordal length (*l*) of the suture line (B). As a series of *x*-coordinate values is not periodic but logically increases (C), such series were detrended by subtracting the expected linear increase in *x* to introduce periodicity to the *x* function (D).

prominent saddle when E_2 is negative (E_2 minimum in Fig. 2D).

Plots of E_2 versus E_1 are effective in depicting differences in the *y* function among taxa (Fig. 2A–C). Most species belonging to the Agoniatitida, Clymeniida or Prolecanitida occupy the region around the origin of the morphospace (Fig. 2A, B), even though the suture shape appears dissimilar among these taxa. The mean shape of synthetic models of the *y* function illustrated at the origin of the morphospace is approximately flat, with little amplitude (see 'mean' in Fig. 2D); i.e. suture shapes surrounding the origin are characterized by small amplitude regardless of the number of the first-order elements. By contrast, both goniatitids and ceratitids cover a wider area of the morphospace (Fig. 2A, B). In the Mesozoic ammonitids, most species belonging to the Lytoceratina and Ammonitina are characterized by a small negative value of E_1, which represents the prominence of the ventrally situated saddle; however, the Phylloceratina, in addition to the goniatitids and ceratitids, cover a wide range of E_1 (Fig. 2C). With regard to ES2, all individuals belonging to the Phylloceratina have positive E_2. Most phylloceratine species have positive E_1 and/or large E_2; this condition indicates that the largest lateral lobe is located at the ventro-lateral portion of the shell.

Analysis of the x′ function

The ES1 is outstanding among eigenshapes, and ES1 and ES2 explain 57.3% and 9.4% of the total variance respectively. Synthetic models of the x' function reconstructed along the eigenshape axes clearly show the close relationship between eigenshape scores and concavity of the model (Fig. 3D). Positive perturbations associated with each eigenshape axis represent the strongly concave shape of the synthetic model; however, the position of the trough in the model is different between large E_1 and large E_2 extremes: it lies toward the umbilicus in the former case.

The distribution of eigenshape scores is different between ammonitids and other ammonoids (Fig. 3A–C): agoniatitids, goniatitids, clymeniids, prolecanitids and ceratitids cover a wide range from the negative to positive E_1 regions of the morphospace, although all have E_1 values below 450 (Fig. 3A, B); by contrast, the Ammonitida occupy the large E_1 area. In particular, the Phylloceratina possess E_1 values greater than 420 (Fig. 3C). This distribution reflects the strongly concave shape of the x' function, as characteristically found in ammonitids.

Discussion

In the context of ammonoid macrotaxonomy, primary sutures – the fundamental sutures formed at the early ontogeny – have attracted greater attention than have adult sutures. The number of primary suture elements, as well as the manner of subsequent introduction of new lobes, has been regarded as an important criterion in subdividing ammonoids into several orders and/or suborders (Schindewolf 1954; Kullmann & Wiedmann 1970; Wiedmann & Kullmann 1981; Korn *et al.* 2003). Comparative anatomy and relevant nomenclature on ammonoid sutures are based on their ontogenetic development rather than geometric similarity. Consequently, the geometric properties of adult sutures have principally inspired studies of functional morphology (Henderson 1984; Jacobs 1990; Daniel *et al.* 1997; Hewitt &

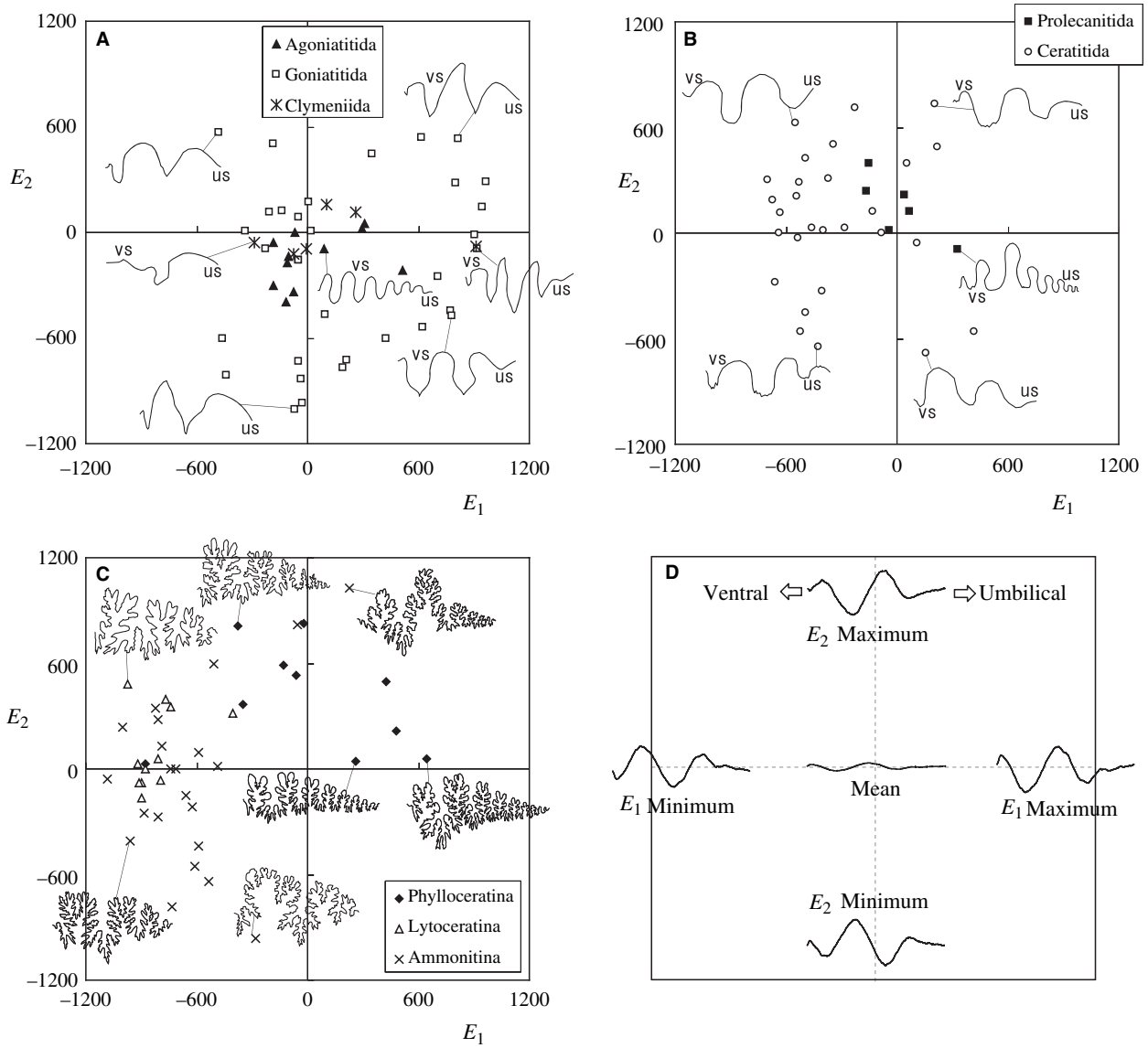

Fig. 3. Results of eigenshape analysis based on the *y* function. A–C, scatter plots of eigenshape scores on the first two eigenshapes, showing examples of selected suture shapes. The position of the ventro-lateral shoulder (vs) and umbilical shoulder (us) are shown in each diagram. A, Agoniatitida, Goniatitida and Clymeniida. B, Prolecanitida and Ceratitida. C, Ammonitida. D, synthetic models visualizing the shape of the *y* function at the extremes of the first two eigenshape axes (maximum and minimum) and for the mean ES1 score.

Westermann 1997; Olóriz *et al.* 1997; Saunders & Work 1997; Hassan *et al.* 2002; Lewy 2002; Pérez-Claros *et al.* 2007) rather than assessments of phylogenetic aspects. The present study revealed differences in occupation pattern in the morphospace of adult sutures among higher taxa of ammonoids.

Analysis of the *y* function revealed that goniatitids and ceratitids cover a wide region of the morphospace (Fig. 2A, B). The area in the morphospace covered by each taxon depends on how many species were sampled; a much larger number of goniatitid and ceratitid species were utilized in this study than were agoniatitids, clymeniids and prolecanitids. Therefore, the result does not necessarily indicate that the Goniatitida and Ceratitida are more disparate than the other Palaeozoic orders, although it does show that both the goniatitid and ceratitid samples accommodate a wide variation in suture shapes surrounding the origin of the morphospace.

By contrast, lytoceratine and ammonitine species have negative E_1 values that are much smaller in value than those of other ammonoids (Fig. 2). The typical lytoceratine and ammonitine sutures develop a prominent saddle near the venter; this feature is less common in other ammonoids (Figs 2, 4). However, the Phylloceratina – the stem group of the Ammonitida – have a wide range in E_1, as do the Triassic ceratitids and Palaeozoic goniatitids (Fig. 2C). In most

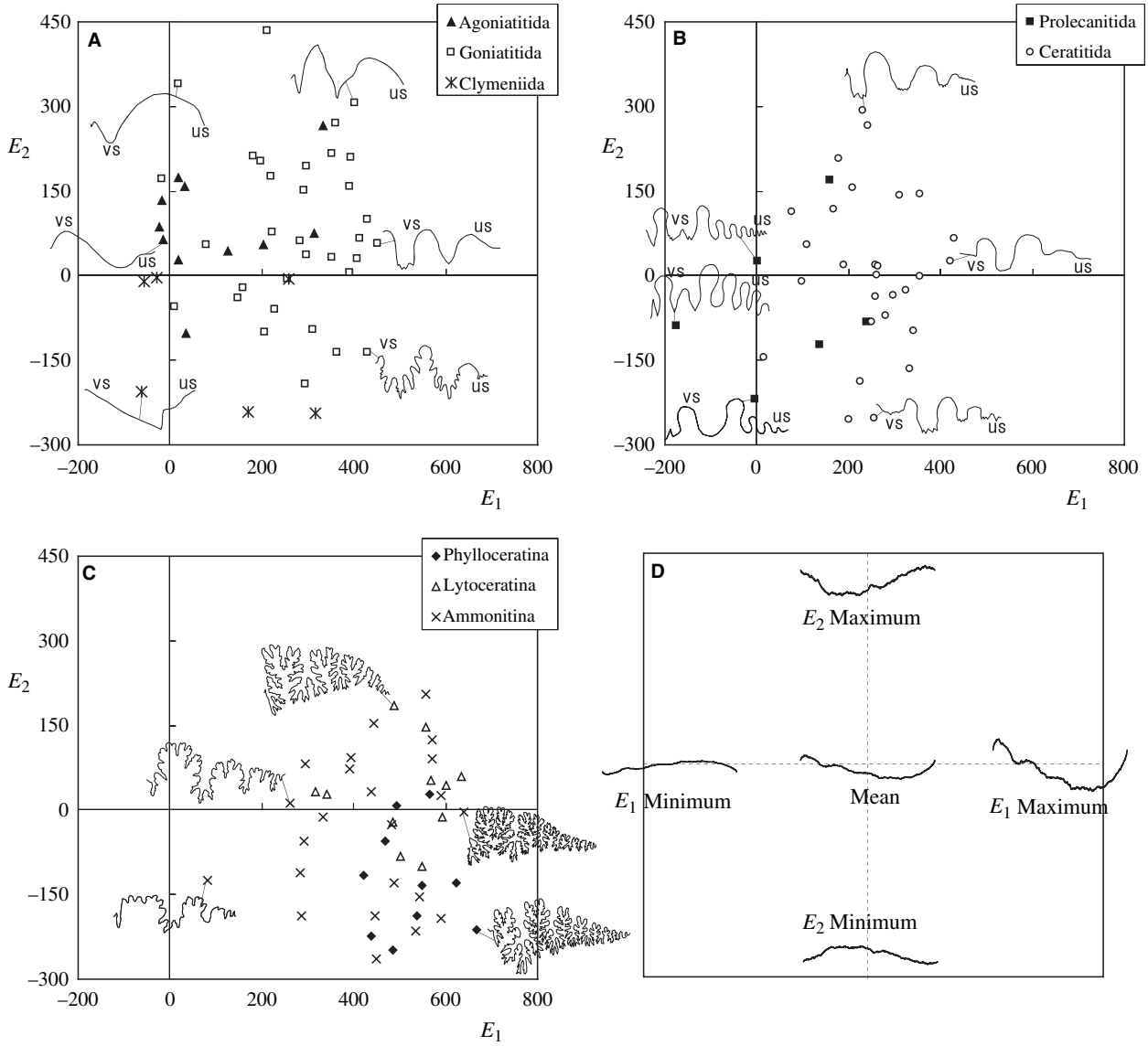

Fig. 4. Results of eigenshape analysis based on the x' function. A–C, scatter plots of eigenshape scores on the first two eigenshapes showing examples of selected suture shapes. The position of the ventro-lateral shoulder (vs) and umbilical shoulder (us) are shown in each diagram. A, Agoniatitida, Goniatitida and Clymeniida. B, Prolecanitida and Ceratitida. C, Ammonitida. D, synthetic models visualizing the shape of the y function at the extremes of the first two eigenshape axes (maximum and minimum) and for the mean ES1 score.

phylloceratine sutures, the largest saddle is found on the lateral flank of the whorl (Fig. 4), whereas it is situated near the venter in the typical lytoceratine and ammonitine sutures. Given that the Ammonitida are derived from the Ceratitida via some phylloceratine species (Shigeta & Weitschat 2004), the result of the eigenshape analysis for the y function seems to reveal a plesiomorphic aspect of adult suture shapes in some phylloceratine species with respect to other ammonitids that possess more highly specialized suture shapes.

Focusing on the x' function, the phylogenetic aspect of the phylloceratine suture appears to contradict the finding obtained from the analysis of the y function. Among the examined ammonoid taxa, ammonitid species (particularly phylloceratine ones) tend to occupy an area near the lower right (large E_1 and small E_2) corner of the morphospace (Fig. 2C), whereas the other ammonoids range from the central region to the left-hand side of the diagram shown in Fig. 2A, B. Therefore, the result of the analysis based on the x' function indicates an apomorphic aspect of phylloceratine sutures; however, unlike the y function, any geometric interpretation based on the x' function is not straightforward. The descriptor of the x' function represents the deviation of the observed x-coordinate of each point from the expected x value of the point, which shows a linear increase.

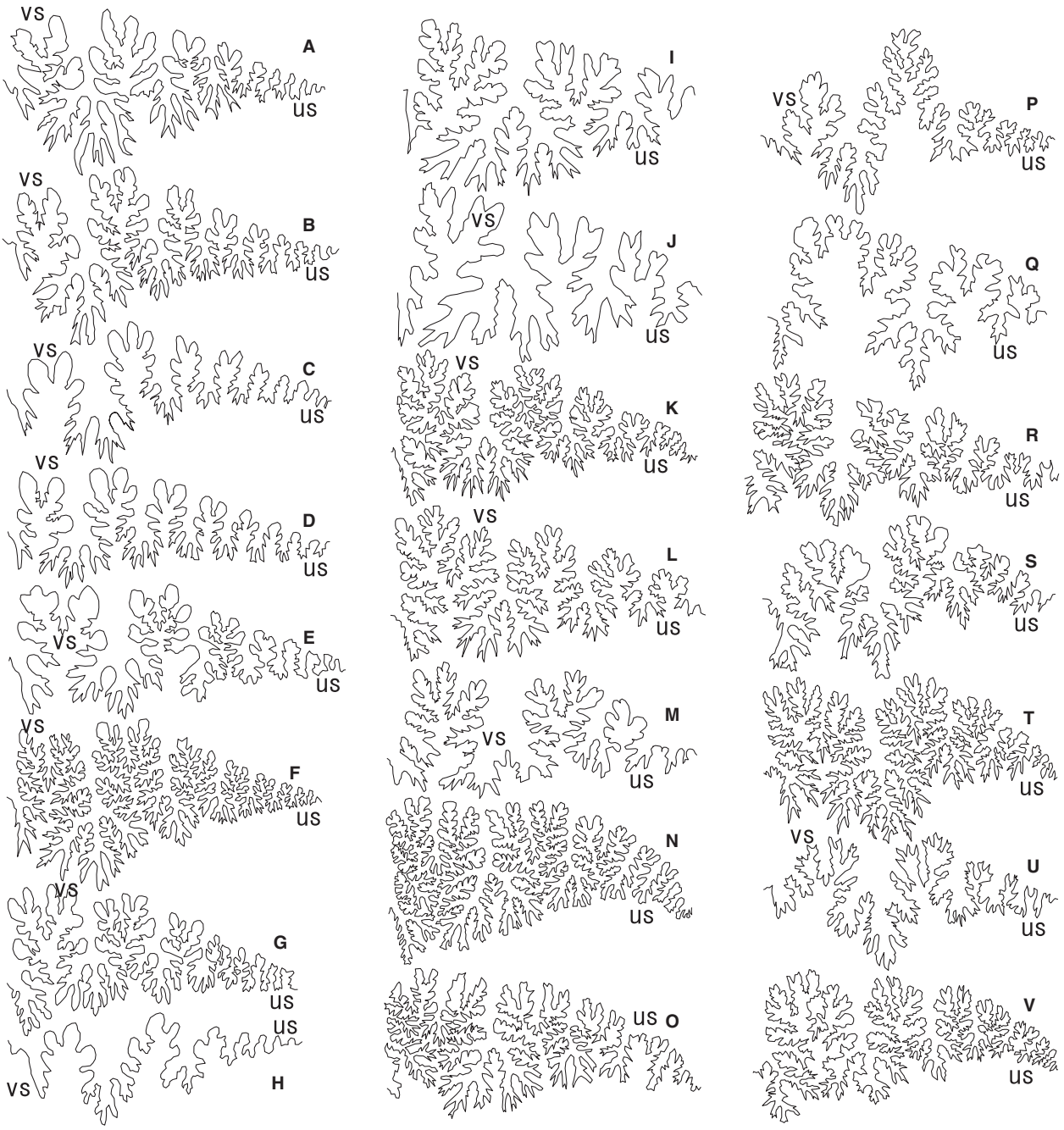

Fig. 5. Traced suture lines in selected ammonitid species. The position of the ventro-lateral shoulder (vs) and umbilical shoulder (us) are shown in each diagram. A, *Phylloceras consanguineum*. B, *Phylloceras* sp. C, *Holcophylloceras* sp. D, *Calliphylloceras* sp. E, *Ptychophylloceras* sp. F, *Hypophylloceras subramosum*. G, *Phyllopachyceras ezoense*. H, *Tragophylloceras ibex*. I, *Pterolytoceras* sp. J, *Argonauticeras* sp. K, *Tetragonites popetensis*. L, *Tetragonites glabrus*. M, *Eotetragonites* sp. N, *Gaudryceras striatum*. O, *Gaudryceras tenuiliratum*. P, *Lissoceras* sp. Q, *Euaspidoceras* sp. R, *Desmoceras latidorsatum*. S, *Hauericeras angustum*. T, *Yokoyamaoceras ishikawai*. U, *Cleoniceras besairiei*. V, *Canadoceras kosmatti*.

To illustrate the nature of the x' function, consider the case of two travellers making their way from the ventral extreme of a suture line to the umbilical extreme via the following different routes: one travelling along the suture line and the other travelling in a straight line. Each travels at a constant speed along the respective route, but both start and arrive at the same time. At a given time point, the former lags behind or moves ahead of the latter in travelling toward the umbilicus: the x' function represents, as it were, the extent to which the former precedes the latter. Therefore, the former lags behind the latter in the concave portion of the model of the x' function, whereas it precedes the latter in the convex portion. The shape of the

model x' function typically observed in ammonitids is characterized by a wide and deep concavity (Fig. 3C, D), thereby indicating that when travelling along the typical ammonitid suture, one slowly approaches the umbilicus in the ventral to lateral portions but accelerates in the umbilical area. This situation is realized when the suture shape is strongly meandering and when the largest suture element develops in the ventrolateral portion rather than near the umbilicus.

This geometric interpretation of the x' function is concordant with the following interpretation based on the y function: the lytoceratine and ammonitine sutures are characterized by a prominent saddle situated near the venter, whereas for phylloceratine sutures the largest lobe tends to occur in this position. In addition, a widely concave model of the x' function is generated if the amplitude of the meandering suture shows a rapid decline near the umbilicus. Indeed, most phylloceratine species develop lobe splitting near the umbilical seam or auxiliary lobes (Arkell *et al.* 1957), which rapidly reduce their amplitude and sinuosity approaching the umbilicus (Fig. 4). It is likely that this feature of phylloceratine sutures results in their models of the x' function having the most strongly concave shapes (Fig. 5), yielding the highest E_1 values among other ammonoids.

In summary, the present eigenshape analyses captured the following differences in adult suture shape between ammonitids and other ammonoids. In comparison with non-ammonitid species, most lytoceratine and ammonitine species developed the largest saddle near the venter, such that the centre of the density or geometric 'centroid' of the suture curve is ventrally situated; however, such an evolutionary novelty was not achieved by the Phylloceratina, a rootstock of other ammonitids. Instead, the largest lobe of the Phylloceratina is located near the venter, as commonly found in ceratitids and Palaeozoic ammonoids. Nevertheless, the Phylloceratina developed complicated ammonitic sutures, as did the Lytoceratina and Ammonitina, and their first-order suture elements are heavily frilled. However, a series of auxiliary elements of phylloceratine sutures, formed by the splitting of an umbilical lobe and typically seen in prolecanitids and some ceratitids, is much less denticulate than the lateral saddles and lobes, meaning that the 'centroid' of the suture curve is located toward the venter.

To summarize the above results and interpretations, the characteristics of ammonitid sutures are not only their conspicuous complexity but also the ventrally situated position of the 'centroid' of the suture curve. Most phylloceratine species seem to have obtained these characteristics in such way that they partly followed the phylogenetic legacy from ancestral ammonoids; however, more derived lytoceratine and ammonitine ammonoids appear to have obtained these characteristics via a more drastic reform. A diagnostic sutural characteristic, appropriate for distinction of the Lytoceratina and Ammonitina from the Phylloceratina, is the incised dorsal lobe (Kullmann & Wiedmann 1970; Shevyrev 2006), rather than features of the external suture. Lobe splitting near the umbilical seam, as seen typically in the Phylloceratina, is also found in the Lytoceratina and Ammonitina (Kullmann & Wiedmann 1970; Wiedmann & Kullmann 1981). Nevertheless, the present analysis indicates that differences in morphological variation can be found among taxa even if the shapes of the external sutures are compared using mature individuals. The several derived characteristics of suture shape that are found in the Lytoceratina and Ammonitina support the phylogenetic hypothesis that they are derivatives of the Phyllocetaina.

The eigenshape-based method introduced above provides a useful tool in defining a morphospace, which accommodates various suture shapes. This paper presents a case study involving comparisons among higher taxa; however, our approach is also applicable to the comparisons among closely related species and to analyses of within-species variation. The present analysis successfully distilled the first-order morphological components from complex suture curves, but we did not address variations in finer structures. Further refinements will expand the utility of our approach for capturing richer structures and the ordination of various shapes in a variety of organisms.

Acknowledgements. – We thank C. Klug and an anonymous referee for their helpful comments on the first draft. Funding of this work was provided in part by a Grant-in-Aid for Scientific Research from the Japan Society for the Promotion of Science (No. 20540457).

References

Allen, E.G. 2006: New approaches to Fourier analysis of ammonoid sutures and other complex, open curves. *Paleobiology 32*, 299–315.

Allen, E.G. 2007: Understanding ammonoid sutures: new insight into the dynamic evolution of Paleozoic suture morphology. *In* Landmann, N.H., Davis, R.A. & Mapes, R.H. (eds.): *Cephalopods Present and Past: New Insights and Fresh Perspectives*, 159–180. Springer-Verlag, Dordrecht.

Arkell, W.J. 1957: Introduction to Mesozoic Ammonoidea. *In* Moore, R.C. (ed.): *Treatise on Invertebrate Paleontology, Volume L*, 81–129. Geological Society of America, Boulder, and University of Kansas Press, Lawrence.

Arkell, W.J., Kummel, B. & Wright, C.W. 1957: Systematic descriptions. *In* Moore, R.C. (ed.): *Treatise on Invertebrate Paleontology, Volume L*, 129–437. Geological Society of America, Boulder, and University of Kansas Press, Lawrence.

Ballantine, C.M. 2007: A mathematical analysis of some indices used to classify ammonite shells. *Lethaia 40*, 197–198.

Batt, R.J. 1991: Sutural amplitude of ammonite shells as a paleoenvironmental indicator. *Lethaia 24*, 219–225.

Bayer, U. 1978: The impossibility of inverted suture lines in ammonites. *Lethaia 11*, 307–313.

Becker, R.T. & Kullmann, J. 1996: Paleozoic ammonoids in space and time. *In* Landman, N., Tanabe, K. & Davis, R.A. (eds): *Ammonoid Paleobiology*, 711–753. Prenum, New York.

Boyajian, G. & Lutz, T. 1992: Evolution of biological complexity and its relation to taxonomic longevity in the Ammonoidea. *Geology 20*, 983–986.

Canfield, D.J. & Anstey, R.L. 1981: Harmonic analysis of cephalopod suture patterns. *Mathematical Geology 13*, 23–35.

Checa, A.G. & García-Ruiz, J.M. 1996: Morphogenesis of the septum in ammonoids. *In* Landman, N., Tanabe, K. & Davis, R.A. (eds): *Ammonoid Paleobiology*, 253–296. Prenum, New York.

Daniel, T.L., Helmuth, B.S., Saunders, W.B. & Ward, P.D. 1997: Septal complexity in ammonoid cephalopods increased mechanical risk and limited depth. *Paleobiology 23*, 470–481.

De Blasio, F.V. 2008: The role of suture complexity in diminishing strain and stress in ammonoid phragmocones. *Lethaia 41*, 15–24.

García-Ruiz, J.M., Checa, A. & Rivas, P. 1990: On the origin of ammonite sutures. *Paleobiology 16*, 349–354.

Gildner, R.F. 2003: A Fourier method to describe and compare suture patterns. *Palaeontologia Electronica 6*, 12 <http://palaeo-electronica.org/palaeo/2003_1/suture/issue1_03.htm>.

Hammer, Ø. 1999: The development of ammonoid septa: an epithelial invagination process controlled by morphogens? *Historical Biology 13*, 153–171.

Hassan, M.A., Westermann, G.E.G., Hewitt, R.A. & Dokainish, M.A. 2002: Finite-element analysis of simulated ammonoid septa (extinct Cephalopoda): septal and sutural complexities do not reduce strength. *Paleobiology 28*, 113–126.

Henderson, R.A. 1984: A muscle attachment proposal for septal function in Mesozoic ammonites. *Palaeontology 27*, 461–486.

Hewitt, R.A. & Westermann, G.E.G. 1986: Function of complexly fluted septa in ammonoid shells. I. Mechanical principles and functional models. *Neues Jahrbuch für Geologie und Paläontologie, Abhandlungen 172*, 47–69.

Hewitt, R.A. & Westermann, G.E.G. 1987: Function of complexly fluted septa in ammonoid shells. II. Septal evolution and conclusions. *Neues Jahrbuch für Geologie und Paläontologie, Abhandlungen 174*, 135–169.

Hewitt, R.A. & Westermann, G.E.G. 1997: Mechanical significance of ammonoid septa with complex sutures. *Lethaia 30*, 205–212.

Hewitt, R.A., Checa, A., Westermann, G.E.G. & Zaborski, P.M. 1991: Chamber growth in ammonites inferred from colour markings and naturally etched surfaces of Cretaceous vascoceratids from Nigeria. *Lethaia 24*, 271–287.

Jacobs, D.K. 1990: Sutural pattern and shell stress in *Baculites* with implications for other cephalopod shell morphologies. *Paleobiology 16*, 336–348.

Korn, D. & Klug, C. 2002: Ammoneae Devonicae. *In* Riegraf, W. (ed.): *Fossilum Catalogus, Animalia I*, 1–375. Backhuys, Leiden.

Korn, D., Ebbighausen, V., Bockwinkel, J. & Klug, C. 2003: The A-mode sutural ontogeny in prolecanitid ammonoids. *Lethaia 46*, 1123–1132.

Kullmann, J. & Wiedmann, J. 1970: Significance of sutures in phylogeny of ammonoidea. *The University of Kansas, Paleontological Contributions 47*, 1–32.

Lehmann, U. 1981: *The Ammonites: Their Life and Their World*, 246 pp. Cambridge University Press, Cambridge.

Lewy, Z. 2002: The function of the ammonite fluted septal margins. *Journal of Paleontology 76*, 63–69.

Lohmann, G.P. 1983: Eigenshape analysis of microfossils: a general morphometric procedure for describing changes in shape. *Mathematical Geology 15*, 659–672.

Lutz, T.M. & Boyajian, G.E. 1995: Fractal geometry of ammonoid sutures. *Paleobiology 21*, 329–342.

MacLeod, N. 1999: Generalizing and extending the eigenshape method of shape space visualization and analysis. *Paleobiology 25*, 107–138.

Manship, L.L. 2004: Pattern matching: classification of ammonitic sutures using GIS. *Paleontologia Electronica 7*, 15 <http://palaeo-electronica.org/paleo/2004_2/suture/issue2_04.htm>.

Miller, A.K., Furnish, W.M. & Schidewolf, O.H. 1957: Paleozoic Ammonoidea. *In* Moore, R.C. (ed.): *Treatise on Invertebrate Paleontology, Volume L*, 11–79. Geological Society of America, Boulder, and University of Kansas Press, Lawrence.

Olóriz, F. & Palmqvist, P. 1995: Sutural complexity and bathymetry in ammonites: fact or artifact? *Lethaia 28*, 167–170.

Olóriz, F., Palmqvist, P. & Pérez-Claros, J.A. 1997: Shell features, main colonized environments, and fractal analysis of sutures in Late Jurassic ammonites. *Lethaia 30*, 191–204.

Olóriz, F., Palmqvist, P. & Pérez-Claros, J.A. 2002: Morphostructural constraints and phylogenetic overprint on sutural frilling in Late Jurassic ammonites. *Lethaia 35*, 158–168.

Pérez-Claros, J.A. 2005: Allometric and fractal exponents indicate a connection between metabolism and complex septa in ammonites. *Paleobiology 31*, 221–232.

Pérez-Claros, J.A., Palmqvist, P. & Olóriz, F. 2002: First and second orders of suture complexity in ammonites: a new methodological approach using fractal analysis. *Mathematical Geology 34*, 323–343.

Pérez-Claros, J.A., Olóriz, F. & Palmqvist, P. 2007: Sutural complexity in Late Jurassic ammonites and its relationship with phragmocone size and shape: a multidimensional approach using fractal analysis. *Lethaia 40*, 253–272.

Saunders, W.B. 1995: The ammonoid suture problem: relationship between shell- and septal thickness and suture complexity in Paleozoic ammonoids. *Paleobiology 21*, 343–355.

Saunders, W.B. & Work, D.M. 1996: Shell morphology and suture complexity in Upper Carboniferous ammonoids. *Paleobiology 22*, 189–218.

Saunders, W.B. & Work, D.M. 1997: Evolution of shell morphology and suture complexity in Paleozoic prolecanitids, the rootstock of Mesozoic ammonoids. *Paleobiology 23*, 301–325.

Saunders, W.B., Work, D.M. & Nikolaeva, S.V. 1999: Evolution of complexity in Paleozoic ammonoid sutures. *Science 286*, 760–763.

Schindewolf, O.H. 1954: On development, evolution, and terminology of the ammonoid suture line. *Bulletin of the Museum of Comparative Zoology at Harvard College 112*, 217–237.

Seilacher, A. 1975: Mechanische Simulation und funcktionelle Evolution des Ammonite-Septems. *Paläontologische Zeitschrift 49*, 268–286.

Seilacher, A. & LaBarbera, M. 1995: Ammonites as Cartesian divers. *Palaios 10*, 493–506.

Shevyrev, A.A. 2006: The cephalopod macrosystem: a historical review, present state of knowledge, and unsolved problem: 3. classification of Bactritoidea and Ammonoidea. *Paleontological Journal 40*, 151–160.

Shigeta, Y. & Weitschat, W. 2004: Origin of the Ammonitina (Ammonoidea) inferred from the internal shell features. *Mitteilungen aus dem Geologisch-Palaontologisches Institut der Universitat Hamburg 88*, 179–194.

Tozer, E.T. 1981: Triassic Ammonoidea: classification, evolution and relationship with Permian and Jurassic forms. *In* House, M.R. & Senior, J.R. (eds): *The Ammonoidea. The Evolution, Classification, Mode of Life and Geological Usefulness of a Major Fossil Group*, 65–100. Academic Press, London.

Ubukata, T. 2004: A three-dimensional digitizing system based on triangulation using multiple viewing images. *Geoscience Reports of Shizuoka University 31*, 65–72 [in Japanese with English abstract and figure captions].

Ward, P.D. 1980: Comparative shell shape distributions in Jurassic–Cretaceous ammonites and Jurassic–Tertiary nautiloids. *Paleobiology 6*, 32–43.

Weitschat, W. & Bandel, K. 1991: Organic components in phragmocones of Boreal Triassic ammonoids: implications for ammonoid biology. *Paläontologische Zeitschrift 65*, 269–303.

Westermann, G.E.G. 1958: The significance of septa and sutures in Jurassic ammonite systematics. *Geological Magazine 95*, 441–455.

Westermann, G.E.G. 1971: Form, structure and function of shell and siphuncle in coiled Mesozoic ammonoids. *Royal Ontario Museum, Life Sciences Contributions 78*, 1–39.

Westermann, G.E.G. 1975: Model for origin, function and fabrication of fluted cephalopod septa. *Paläontologische Zeitschrift 49*, 235–253.

Wiedmann, J. & Kullmann, J. 1981: Ammonoid sutures in ontogeny and phylogeny. *In* House, M.R. & Senior, J.R. (eds): *The Ammonoidea: the Evolution, Classification, Mode of Life and Geological Usefulness of a Major Fossil Group*, 215–255. Academic Press, New York.

Wright, C.W., Callomon, J.H. & Howarth, M.K. 1996: Ammonoidea Volume 4. *In* Kaesler, R.L. (ed.): *Treatise on Invertebrate Paleontology, Volume L*, Revised, 1–362. Geological Society of America, Boulder.

Zahn, C.T. & Roskies, R.Z. 1972: Roskies, Fourier descriptors for plane closed curves. *IEEE Transactions, Computers C-21*, 269–281.